Ultrasound elasticity of diamond at gigapascal pressures

Qingyang Hu[a,b], Baosheng Li[c,1], Xiang Gao[a], Yan Bi[a], Lei Su[a], and Ho-kwang Mao[a,1]

[a]Center for High Pressure Science and Technology Advanced Research, Beijing 100094, P. R. China; [b]Center for Excellence in Deep Earth Science, Guangzhou Institute of Geochemistry, Chinese Academy of Sciences, Guangzhou 510640, P. R. China; and [c]Department of Geosciences, Stony Brook University, Stony Brook, NY 11794

Contributed by Ho-kwang Mao; received November 5, 2021; accepted November 9, 2021; reviewed by Frédéric Decremps, Larissa Dobrzhinetskaya, and Yongjun Tian

Diamond is the hardest known material in nature and features a wide spectrum of industrial and scientific applications. The key to diamond's outstanding properties is its elasticity, which is associated with its exceptional hardness, shear strength, and incompressibility. Despite many theoretical works, direct measurements of elastic properties are limited to only ∼1.4 kilobar (kb) pressure. Here, we report ultrasonic interferometry measurements of elasticity of void-free diamond powder in a multianvil press from 1 atmosphere up to 12.1 gigapascal (GPa). We obtained high-accuracy bulk modulus of diamond as K_0 = 439.2(9) GPa, K_0' = 3.6(1), and shear modulus as G_0 = 533(3) GPa, G_0' = 2.3(3), which are consistent with our first-principles simulation. In contrast to the previous experiment of isothermal equation of state, the K_0' obtained in this work is evidently greater, indicating that the diamond is not fully described by the "*n-m*" Mie–Grüneisen model. The structural and elastic properties measured in this work may provide a robust primary pressure scale in extensive pressure ranges.

diamond | ultrasonic inteferometry | elasticity | high pressure

The extraordinary mechanical properties of diamond make it an unsurpassed material in cutting, shaping, and compressing hard substances. To date, a large amount of work has aimed to remedy the drawbacks of diamond as a superhard material in the context of industrial implications (1). For instance, the thermal stability, elastic deformability, and toughness of diamond can be improved by synthesizing a nanoscale diamond crystal using high-pressure apparatus (2–6). For such implications, its high-pressure elasticity plays a critical role, and its underlying stiffening mechanism will, in turn, guide the design for better nanoscale diamond.

Diamond is a high-pressure allotrope of carbon. Under high-pressure conditions, the structure of diamond is constructed through a martensitic process in which the sp^3 carbon bonding is formed along a specific shear direction (7, 8). In the opposite, the procedure to break the sp^3 bonding (e.g., the transformation from diamond to graphite) is usually indirect and kinetically inhibited (9). The formation and alignment of sp^3 carbon bonding are the signatures of diamond, whose covalent nature governs its elastic properties. A number of theoretical works were pioneered to calculate the high-pressure elasticity of diamond. Tse et al. calculated the equation of state of diamond to terapascal pressure and temperature up to its melting curve and suggested that diamond is a well-defined covalent solid under such extreme conditions (10). Núñez Valdez et al. calculated the thermoelectricity of diamond to 500 GPa and predicted that the elastic property of diamond becomes increasingly anisotropic at high pressures (11). In stark contrast, experimental works are scarce, especially on the in situ elasticity of compressed diamond. Previously, single-crystal diamond was compressed in a diamond anvil cell (DAC) by Occelli et al., who confirmed that diamond is a Grüneisen solid up to at least 140 GPa and exhibited strengthened covalent bonding. The latest high-pressure, elasticity experiment of diamond, as far as we have investigated, was by McSkimin and Andreatch 40 y ago, who measured the ultrasonic wave velocities up to ∼0.14 GPa (12) and calculated K_0 = 442(11) GPa, K_0' = 4.03(16). Data points on the experimental elastic modulus at gigapascal pressure range is still rare, and they are in urgent need to understand the evolution of diamond elasticity under external stress.

The challenges to perform high-pressure elasticity experiment for diamond, beyond a doubt, stem from its intrinsic properties. Diamond is the key component of DAC, the main instrument for high-pressure research, and thus interferometric measurements, such as Brillouin scattering and ultrasonic interferometry, in a DAC, are impractical because of the interference of the anvils. The experiment using multianvil, high-pressure press is among the few solutions. Since the velocities of compressional wave (V_P, >18 km/s) and shear wave (V_S, >12 km/s) of diamond are very high, a large sample size is required in order to separate the echo from the reference (namely, the buffer rod) signals. The sample assembly limits the achievable pressure to ∼10 GPa. Along with the compression tool, we also developed an ultrasonic interferometry coupled with multianvil apparatus, dedicated for measuring polycrystalline elasticity under high pressure (13). The system has successfully obtained high-accuracy, elastic parameters for a variety of solids and liquids (14–17). Since diamond is extremely incompressible, such that the travel time change within this pressure range is tiny, our measurement will challenge the limit of instrumental precision using the current setups.

The focus of this work is to measure the high-pressure, elastic properties of diamond. High-quality elasticity data and their pressure derivatives are the prerequisite to establish a primary

Significance

The exceptional hardness of diamond makes it an unmatched material for compressing and mechanical processing. For the same reason, compressing diamond and measuring its high-pressure, elastic properties turns out to be a very challenging task. Combining the ultrasonic interferometry and multianvil press, we extended the research forefront of diamond's elasticity from kilobar to gigapascal pressures and showed that diamond becomes increasingly compressible, reaching agreement with theory. The results also point out the unique potential of diamond in providing an accurate, absolute pressure standard up to the terapascal region, which will be the basis cornerstone of the extensive, high-pressure sciences.

Author contributions: Q.H. and H.-k.M. designed research; Q.H., B.L., and X.G. performed research; Y.B. and L.S. contributed new reagents/analytic tools; Q.H. and B.L. analyzed data; and Q.H. and H.-k.M. wrote the paper.

Reviewers: F.D., University of Pierre and Marie Curie; L.D., University of California Riverside; and Y.T., Yanshan University.

The authors declare no competing interest.

[1]To whom correspondence may be addressed. Email: maohk@hpstar.ac.cn or baosheng.li@stonybrook.edu.

Published December 14, 2021.

PHYSICS

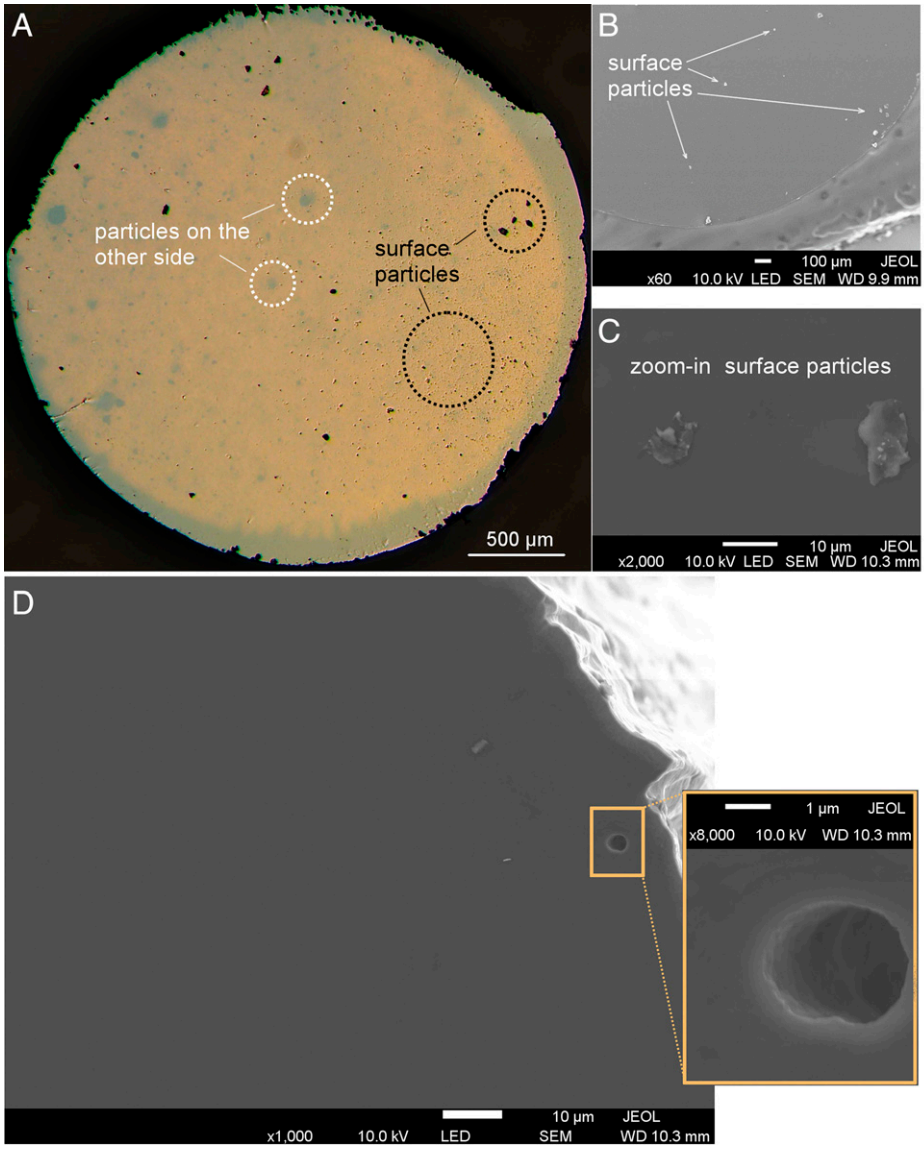

Fig. 1. Optical and scanning electron microscope (SEM) images of void-free diamond samples. (*A*) A microscope image. The small dark particles are not pores under higher-resolution SEM image. (*B*) A secondary electron image (ESI) showing the surface particles. (*C*) A zoom-in of ESI surface particles. (*D*, *Inset*) Surface pores of ~1 μm were observed only by the edge of the specimen. Abbreviations: LED, light emitting diode; WD, working distance.

pressure scale for high-pressure sciences (18). Previous experiments obtained primary scale up to 120 GPa from static compression (19, 20) and multimegabar pressures from dynamic compression (21). Since diamond is thermodynamically stable in terapascal pressure range (22), it is possible to create a diamond primary pressure scale for much extended pressures. The results will be a solid anchor for pressure gauges, for example, ruby fluorescence (23), the Raman edge of diamond anvil (24), and the X-ray diffraction of metal (25).

Results and Discussion

The starting sample is void-free polycrystalline diamond cylinders of 3 mm in diameter and length (26). It features a compact, poreless, and somewhat tedious surface (Fig. 1) that is ideal for measuring wave velocities. We performed two runs of the experiment using ultrasonic interferometry. Ultrasonic measurement was performed using a pulse echo overlap method of ultrasonic interferometry (27) in a Kawai-type, multianvil apparatus (USCA-1000) installed in the High Pressure Laboratory of Stony Brook University. Details of experiment settings have been described in previous publications (13, 28, 29).

We employed a dual-mode $LiNbO_3$ transducer (Boston-Optics) with a resonance frequency of 50 MHz for *P* wave and 30 MHz for *S* wave as both transmitter and receiver of a broadband ultrasonic signal (20 to 70 MHz). The cylindrical polycrystalline diamond samples were shaped to 3.0 mm in diameter and 2.55 to 2.65 mm in length and were positioned approximately at the center of a 14-mm MgO octahedron. A polycrystalline Al_2O_3 rod (Coors 998, diameter 3.2 mm and 3.75 mm long) was inserted into the MgO octahedron to contact the front surface of the sample and served as an acoustic buffer rod to help propagate high-frequency, ultrasonic waves into the sample. A layer of 2-μm-thick gold foil was used as coupling agent at the sample and buffer rod interface (as well as at the interface between the buffer rod and tungsten carbide anvil) to maximize the propagation of acoustic energy into the sample (Fig. 2). To reduce the deviatoric stresses during acoustic measurement at high pressure, the back surface and the surrounding of the polycrystalline diamond sample were supported

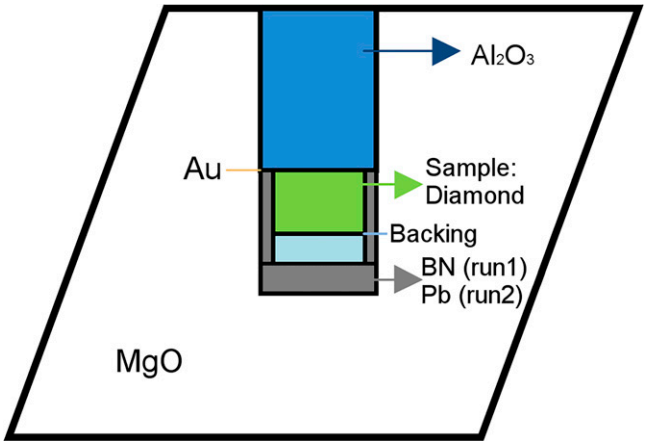

Fig. 2. Cross-section of the cell assembly used in the multianvil experiment.

by soft materials (Run #1, BN; Run #2, Pb). As indicated by direct measurements after high-pressure experiments, both samples remained at their original lengths before experiments, suggesting that only elastic deformation had occurred in the course of the experiments.

The pressure was measured using a recently developed Wang–Chen–Qi acoustic pressure scale (30). The sample length (l) at high pressures was obtained from the measured P and S wave travel times of the polycrystalline diamond sample (t_P and t_S) and its initial density (ρ_0) and length (l_0) at ambient conditions or the so-called Cook's method (31) (details in *Methods*). The results of travel times, sample lengths, P and S wave velocities (V_P and V_S), densities (ρ), and bulk (K) and shear (G) modulus from the current experiments are all listed in Table 1. The absolute wave velocities of V_P and V_S from the two experiments

Table 1. Results of ultrasonic interferometry experiments

Pressure (GPa)	t_P (ms)	t_S (ms)	l (mm)	ρ (g/cm^3)	V_P (km/s)	V_S (km/s)	K (GPa)	G (GPa)
Run 1								
0.0	0.2820	0.4135	2.563	3.500	18.18	12.40	439.3	537.9
3.3	0.2800	0.4116	2.557	3.526	18.26	12.42	450.3	544.2
5.4	0.2784	0.4106	2.553	3.542	18.34	12.43	461.1	547.7
6.6	0.2774	0.4088	2.550	3.552	18.39	12.48	463.7	553.0
7.6	0.2766	0.4082	2.549	3.560	18.43	12.49	468.8	555.1
8.8	0.2760	0.4082	2.547	3.568	18.45	12.48	474.4	555.5
9.7	0.2754	0.4068	2.545	3.575	18.48	12.51	474.9	559.7
10.7	0.2746	0.4062	2.543	3.583	18.52	12.52	480.2	561.7
11.1	0.2750	0.4064	2.543	3.584	18.49	12.51	477.4	561.3
11.0	0.2746	0.4062	2.543	3.585	18.52	12.52	480.3	561.8
10.2	0.2752	0.4068	2.544	3.578	18.49	12.51	476.8	559.9
9.4	0.2758	0.4070	2.546	3.573	18.46	12.51	472.0	559.0
8.7	0.2762	0.4080	2.547	3.567	18.44	12.48	471.9	556.0
8.4	0.2764	0.4082	2.547	3.565	18.43	12.48	470.8	555.3
6.2	0.2776	0.4088	2.551	3.549	18.38	12.48	461.8	552.9
Run 2								
6.6	0.2764	0.4064	2.534	3.552	18.34	12.41	465.1	547.2
7.1	0.2760	0.4062	2.534	3.556	18.36	12.41	468.0	547.9
7.8	0.2755	0.4052	2.532	3.562	18.38	12.44	469.0	550.9
9.3	0.2750	0.4046	2.530	3.573	18.40	12.44	471.7	553.2
10.3	0.2741	0.4036	2.528	3.581	18.44	12.46	476.4	556.3
11.4	0.2733	0.4030	2.526	3.589	18.48	12.47	481.7	558.4
12.1	0.2728	0.4024	2.524	3.595	18.51	12.48	484.2	560.3

Errors for data are the following: ±0.0002 ms for t_P and t_S; ±0.0002 for length l; ±0.04 km/s for V_P; ±0.024 km/s for V_S; ~±1.4 GPa for K; and ±2.1 GPa for G.

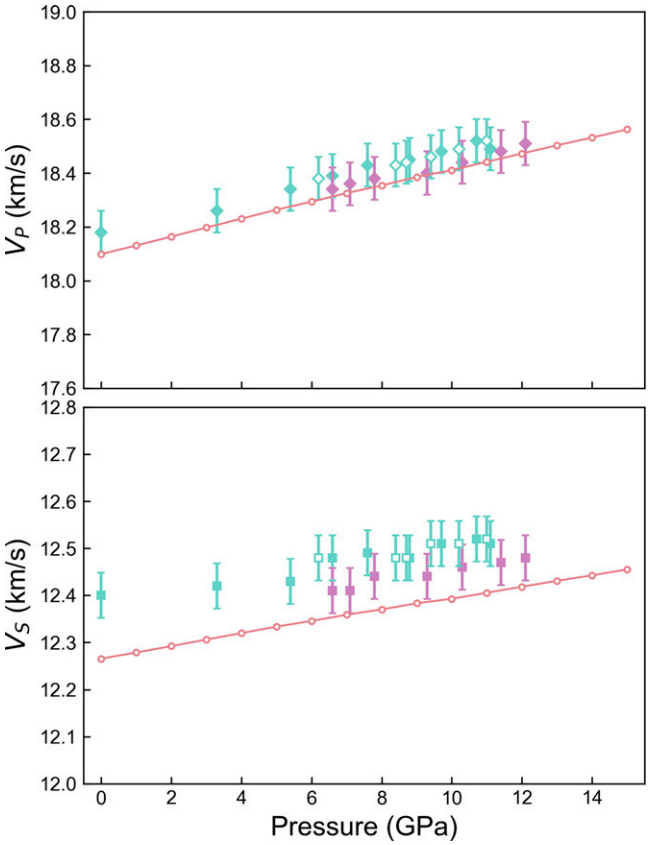

Fig. 3. Sound velocities with change of pressure. Results from experiment are in solid or open (decompression) symbols with error bar. Cyan or magenta symbols are data taken from run 1 or run 2, respectively. The red curve with open circles stands for DFT calculation.

are in agreement within ~0.5%. They also match well with our density functional theory (DFT) simulation (Fig. 3; simulation details in the *Methods*). We noticed that the V_S from our DFT simulation systematically shift to higher values (e.g., DFT V_S = 12.38 km/s at 0 GPa; Fig. 3). This is because the simulation regarded an ideal, defect-free diamond lattice, and therefore, our calculated crystal lattice is ~1.5% denser. However, such systematic uncertainty, after propagation, is only around 1%, compared to our experiment, and have been reasonably covered by the error bars.

We continued to fit the velocity data from compression and decompression from the experiment (Fig. 4). Here, Run #1 yielded K_0 = 439.4(9) GPa, K_0' = 3.72(7), G_0 = 536.7(19) GPa, and G_0' = 2.33(19), while fitting to those from Run #2 resulted in K_0 = 440.5(14) GPa, K_0' = 3.52(10), G_0 = 531.5(21) GPa, and G_0' = 2.37(19). The values of K_0 and G_0 from these fittings are consistent with literature data (10, 32) and our DFT simulation (see Table 1 and Fig. 4). For the two runs of experiments, the slightly higher K_0' from Run #1 is believed to be caused by a more rigid assembly using BN to surround the sample compared to the use of Pb in Run #2. The rigidity of surrounding materials affects the yield strength, which imposes a minor effect on the measuring of wave velocity at low pressures. We also noticed that the bulk modulus K from our DFT simulation is slightly higher than that from experiment (e.g., K_0 = 450.6 GPa from DFT; Fig. 4), which is believed to be a systematic shift propagated from the above wave velocities. It is worth mentioning that K_0' obtained from experiments are far from reaching an agreement with literature. The pioneered, ultrasonic experiment by McSkimin and Andreach (12)

PHYSICS

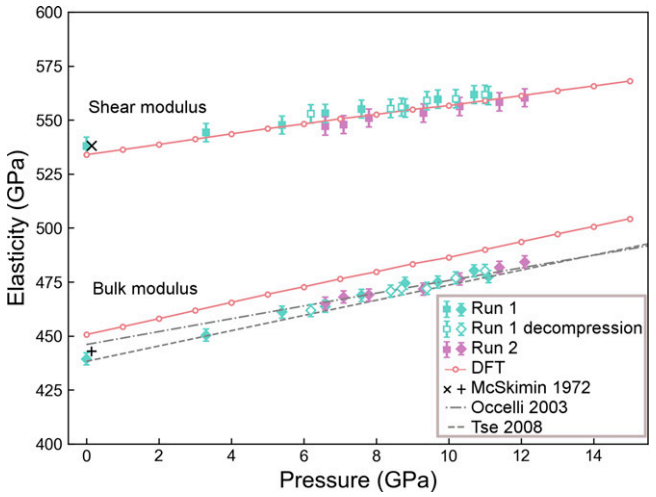

Fig. 4. Pressure versus bulk modulus and shear modulus. Experimental data are plotted in symbols with error bar. The bulk modulus and shear modulus data points are represented by squares or diamonds, respectively. The red curve with open circles is from DFT calculation.

determined $K_0' = 4.03(16)$, which is much greater than the one [$K_0' = 3.0(1)$] derived from the *P-V* equation of state of single-crystal diamond (32). Our value is in between the two and closest to the K_0' predicted from DFT (10). Since K_0' is the signature value for solid compressibility, our experiment confirms that diamond becomes increasingly compressible under pressure. However, the elasticity is not simply described by the "*n-m*" Mie's potential model (33), in which K_0' is a function of the thermodynamic Grüneisen parameter γ_{th} through $K_0' = 2\gamma_{th} + 1$ with $\gamma_{th} = 0.74$ of diamond at ambient conditions (34).

With high-accuracy, elastic parameters, it is possible to integrate pressure through the definition of bulk modulus:

$$\frac{dP_{abs}}{dV} = -\frac{K}{V}, \qquad [1]$$

where P_{abs} is the absolute pressure determined by integrating volume. We cross-checked the P_{abs} from the elasticity of diamond and the standard acoustic pressure scale in Fig. 5, *Left*. The minor error generated in the experiment is negligible throughout the pressure range we have investigated, suggesting that diamond's strong potential is a primary scale in extended pressure ranges. Although the uppermost pressure in the current work is constrained by the multianvil assembly, it is possible to derive elastic parameters from the relation with optical properties, for instance, through the valence force field theory (35, 36).

We also plotted the K versus diamond Raman frequency (ω_0) in Fig. 5, *Right*. We shall note that the slope of K-ω_0 plays a pivot role as K' makes a major contribution to the error of propagated pressure. Since the K values from our DFT calculation are systematically higher, we multiplied all calculated K by a fix number (0.98 in this study), such that, at ambient pressure, K_0 from the DFT calculation is equal to our experiment. The ω_0 values of this work were calculated from the P-ω_0 relation on the basis of previous diamond Raman data (24), and this will allow direct comparison of K-ω_0 slopes between this work and the literature. The K-ω_0 by Aleksandrov et al. [$K' = 1.9(3)$] (37) is quite off from our experimental data. In comparison, the trend of K-ω_0, established by Occelli et al., is much more consistent with our experiment because of their greater K' value [$K' = 3.0(1)$] (32). The K values in both literature works were derived from the equations of state, which is very sensitive to the value of K' or the compressibility of diamond. For this reason, extrapolation beyond the range of equitation of state is likely to inflate uncertainties. Our results also suggested that the K-ω_0 relation from the DFT simulation has better agreement with the experiment up to 12 GPa, proving that diamond is a typical covalent solid under compression. The coupling of the experiment and first-principles simulation at higher pressure may require a thorough evaluation in a future study.

Conclusion

Recent progress in ultrasonic interferometry helped us to increase the margins of high-pressure elasticity in diamond from kilobar to gigapascal level. Our in situ wave velocity measurements confirmed that the covalent bonding of diamond is strengthened under pressure (32). In addition, information about sound velocities of compressed diamond will benefit planetary research for carbon-enriched exoplanets like 55

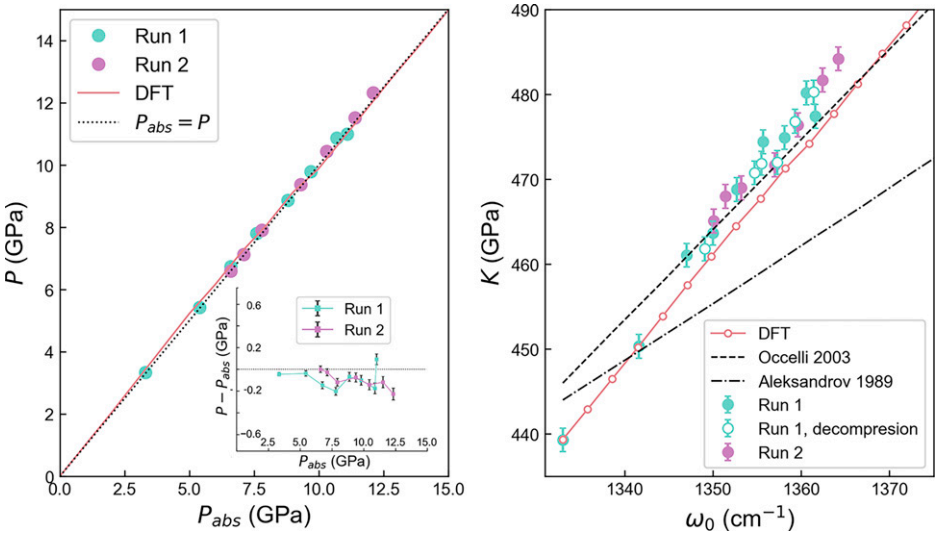

Fig. 5. Diamond as a primary pressure scale. (*Left*) The absolute pressure (P_{abs}) from integration versus the pressure inferred from the Wang–Chen–Qi acoustic pressure scale (30). The inset figure is the difference of P_{abs} and the acoustic pressure scale (P-P_{abs}) with error bars. The difference is below 0.2 GPa. (*Right*) Diamond Raman frequency versus bulk modulus. The Raman frequencies of our experiment were calculated from pressure (44) and were compared against with literature data of Occelli (32) and Aleksandrov (37).

Cancri e (38), who may feature a shell of diamond-dominated mantle.

From DAC to the sintered diamond cube for multianvil press, proceedings of high-pressure science rely heavily on the use of diamond. Not only being the ideal compression tool, diamond Raman edge is one of the most popular pressure gauges for DAC users. However, it has been a long pursuit for scientists to develop a primary pressure scale to multimegabar pressure from the static compression experiment that can be compared with dynamic compression (21) and be anchored to a variety of optical or X-ray gauges. A small, individual diamond crystal will be such a candidate because of its unprecedent thermal stability and incompressibility. Our attempt to measure its ultrasonic elasticity will be the very first attempt for this goal. However, more work is needed to understand how elasticity properties can be obtained at such pressure conditions, as well as the thermoelasticity of diamond as a function of combined temperature and pressure.

Methods

Pressure Scale in Ultrasonic Interferometry Experiment. The Wang–Chen–Qi acoustic pressure scale used an empirical equation:

$$P = 249.7(1 - t_S/t_{S0}),$$

where t_{S0} and t_S are the shear wave travel time of the polycrystalline Al_2O_3 acoustic buffer rod at ambient and high pressure, respectively. This pressure scale can be used not only for the determination of pressure during compression but also for decompression. According to Wang et al. (30), the pressures determined using this approach have an error of ±0.2 GPa.

The Cook's Method. In Cook et al. (31), the change of sample length is described by the sound wave travel time: t_P and t_S. The full expression is below:

$$\frac{l_0}{l} = 1 + \frac{1 + \alpha\gamma T}{12\rho_0 l_0^2} \int \frac{dP}{1/t_P^2 - 4/3t_S^2},$$

where α is the thermal expansion, γ is the Grüneisen parameter, and T is temperature. The densities at high pressure were obtained through $\rho = \rho_0(l_0/l)^3$, with which the elastic K and G were calculated using $K = \rho(V_P^2 - 4V_S^2/3)$ and $G = \rho V_S^2$. In all these data analyses, a zero-pressure density of 3.50 g/cm^3 was used. To derive the pressure derivatives of the K and G, the experimental data at all pressures were fit to the third-order finite strain equations (39).

$$\rho V_P^2 = (1 - 2\varepsilon)^{(5/2)}(L1 + L2\varepsilon),$$

$$\rho V_S^2 = (1 - 2\varepsilon)^{(5/2)}(M1 + M2\varepsilon),$$

where $\varepsilon = (1/2)\,[1 - (\rho/\rho_0)^{(2/3)}]$, and the coefficients $L1$, $L2$, $M1$, and $M2$ are related to the bulk and shear moduli (K_0 and G_0) and their pressure derivatives (K_0' and G_0') at ambient conditions, $L1 = K_0 + 4G_0/3$, $L2 = 5L1 - K_0(3K_0' + 4G_0')$, $M1 = G_0$, and $M2 = 5G_0 - 3K_0G_0'$.

First-principles Simulation. Elastic properties of diamond were calculated under the framework of DFT implemented in the Vienna Ab initio Simulation Package ver. 5.3.4 (VASP [https://www.vasp.at/]) code (40). We chose hard pseudopotentials for C ($2s^22p^2$). The exchange correlation energy is parameterized by functionals of generalized gradient approximation by Perdew, Burke, and Ernzerhof, revised for solid (41). We employed a plane wave basis set cutoff of 1,000 eV. The Brillouin zone was sampled by a k-points mesh equally spaced by 0.2 Å^{-1}. We first performed full geometric relaxation on a 2 × 2 × 2 supercell (conventional lattice, 64 C atoms). The purpose of using supercell is to minimize the periodic size effect. The relaxation achieved the convergence of 1×10^{-3} eV · Å^{-1} for interatomic forces. We then calculated the 0-K isothermal elastic constant matrix using the strain–stress relation (42) and derived the elastic properties (K and G) by the Voigt–Reuss–Hill averaging scheme (43).

Data Availability. All study data are included in the main text.

ACKNOWLEDGMENTS. A portion of simulation was conducted at the Hefei Advanced Computing Center. Q.H. is supported by the China Academy Engineering Physics Research Project (Grant CX20210048) and a Tencent Xplorer prize. The work is also partially supported by National Natural Science Foundation of China Grant U1930401.

1. Y. Zhang, K. Y. Rhee, D. Hui, S.-J. Park, A critical review of nanodiamond based nanocomposites: Synthesis, properties and applications. *Compos. B Eng.* **143**, 19–27 (2018).
2. Q. Huang *et al.*, Nanotwinned diamond with unprecedented hardness and stability. *Nature* **510**, 250–253 (2014).
3. A. Banerjee *et al.*, Ultralarge elastic deformation of nanoscale diamond. *Science* **360**, 300–302 (2018).
4. A. Nie *et al.*, Approaching diamond's theoretical elasticity and strength limits. *Nat. Commun.* **10**, 5533 (2019).
5. Y. Yue *et al.*, Hierarchically structured diamond composite with exceptional toughness. *Nature* **582**, 370–374 (2020).
6. B. Xu, Y. Tian, Diamond gets harder, tougher, and more deformable. *Matter Radiat. Extreme.* **5**, 068103 (2020).
7. H. Tang *et al.*, Revealing the formation mechanism of ultrahard nanotwinned diamond from onion carbon. *Carbon* **129**, 159–167 (2018).
8. S.-C. Zhu, Q.-Y. Hu, Unraveling the structural transition mechanism of room-temperature compressed graphite carbon. *Phys. Chem. Chem. Phys.* **23**, 20560–20566 (2021).
9. E. O'Bannon *et al.*, The transformation of diamond to graphite: Experiments reveal the presence of an intermediate linear carbon phase. *Diam. Relat. Mater.* **108**, 107876 (2020).
10. J. Tse, W. Holzapfel, Equation of state for diamond in wide ranges of pressure and temperature. *J. Appl. Phys.* **104**, 043525 (2008).
11. M. Núñez Valdez, K. Umemoto, R. M. Wentzcovitch, Elasticity of diamond at high pressures and temperatures. *Appl. Phys. Lett.* **101**, 171902 (2012).
12. H. J. McSkimin, P. Andreatch Jr., Elastic moduli of diamond as a function of pressure and temperature. *J. Appl. Phys.* **43**, 2944–2948 (1972).
13. B. Li, R. C. Liebermann, Study of the Earth's interior using measurements of sound velocities in minerals by ultrasonic interferometry. *Phys. Earth Planet. Inter.* **233**, 135–153 (2014).
14. T. Chen *et al.*, Tracking silica in Earth's upper mantle using new sound velocity data for coesite to 5.8 GPa and 1073 K. *Geophys. Res. Lett.* **44**, 7757–7765 (2017).
15. N. Cai, T. Chen, X. Qi, B. Li, Elastic anomalies across phase transitions of praseodymium to 12 GPa. *J. Appl. Phys.* **124**, 185901 (2018).
16. X. Qi, N. Cai, S. Wang, B. Li, Thermoelastic properties of tungsten at simultaneous high pressure and temperature. *J. Appl. Phys.* **128**, 105105 (2020).
17. F. Decremps *et al.*, Sound velocity and equation of state in liquid cesium at high pressure and high temperature. *Phys. Rev. B* **98**, 184103 (2018).
18. C.-S. Yoo, Chemistry under extreme conditions: Pressure evolution of chemical bonding and structure in dense solids. *Matter Radiat. Extreme.* **5**, 018202 (2020).
19. M. Murakami, N. Takata, Absolute primary pressure scale to 120 GPa: Toward a pressure benchmark for Earth's lower mantle. *J. Geophys. Res. Solid Earth* **124**, 6581–6588 (2019).
20. C.-S. Zha, H. Mao, R. J. Hemley, Elasticity of MgO and a primary pressure scale to 55 GPa. *Proc. Natl. Acad. Sci. U.S.A.* **97**, 13494–13499 (2000).
21. D. E. Fratanduono *et al.*, Establishing gold and platinum standards to 1 terapascal using shockless compression. *Science* **372**, 1063–1068 (2021).
22. A. A. Correa, S. A. Bonev, G. Galli, Carbon under extreme conditions: Phase boundaries and electronic properties from first-principles theory. *Proc. Natl. Acad. Sci. U.S.A.* **103**, 1204–1208 (2006).
23. G. Shen *et al.*, Toward an international practical pressure scale: A proposal for an IPPS ruby gauge (IPPS-Ruby2020). *High Press. Res.* **40**, 299–314 (2020).
24. Y. Akahama, H. Kawamura, Pressure calibration of diamond anvil Raman gauge to 410 GPa. *J. Phys. Conf. Ser.* **215**, 012195 (2010).
25. Y. Fei *et al.*, Toward an internally consistent pressure scale. *Proc. Natl. Acad. Sci. U.S.A.* **104**, 9182–9186 (2007).
26. H. Wang *et al.*, Synthesizing bulk polycrystalline diamond by method of direct phase transition. *Diamond Abrasive Engineer.* **38**, 1–6 (2018).
27. E. P. Papadakis, Ultrasonic phase velocity by the pulse-echo-overlap method incorporating diffraction phase corrections. *J. Acoust. Soc. Am.* **42**, 1045–1051 (1967).
28. B. Li, I. Jackson, T. Gasparik, R. C. Liebermann, Elastic wave velocity measurement in multi-anvil apparatus to 10 GPa using ultrasonic interferometry. *Phys. Earth Planet. Inter.* **98**, 79–91 (1996).
29. B. Li, K. Chen, J. Kung, R. Liebermann, D. Weidner, Sound velocity measurement using transfer function method. *J. Phys. Condens. Matter* **14**, 11337–11342 (2002).
30. X. Wang *et al.*, Acoustic travel time gauges for in-situ determination of pressure and temperature in multi-anvil apparatus. *J. Appl. Phys.* **118**, 065901 (2015).
31. R. K. Cook, Variation of elastic constants and static strains with hydrostatic pressure: A method for calculation from ultrasonic measurements. *J. Acoust. Soc. Am.* **29**, 445–449 (1957).
32. F. Occelli, P. Loubeyre, R. LeToullec, Properties of diamond under hydrostatic pressures up to 140 GPa. *Nat. Mater.* **2**, 151–154 (2003).
33. J.-P. Poirier, *Introduction to the Physics of the Earth's Interior* (Cambridge University Press, Cambridge, UK, ed. 2, 2000).

34. J. E. Field, *The Properties of Natural and Synthetic Diamond* (Academic Press, London, UK, 1997).
35. R. Vogelgesang, A. K. Ramdas, S. Rodriguez, M. Grimsditch, T. R. Anthony, Brillouin and Raman scattering in natural and isotopically controlled diamond. *Phys. Rev. B Condens. Matter* **54**, 3989–3999 (1996).
36. Q. Hu, H.-k. Mao, Born's valence force-field model for diamond at terapascals: Validity and implications for the primary pressure scale. *Matter Radiat. Extreme.* **6**, 068403 (2021).
37. I. V. Aleksandrov *et al.*, Diamond and cubic boron nitride under high pressure: Raman scattering, equation of state and high pressure scale. *High Press. Res.* **1**, 333–336 (1989).
38. N. Madhusudhan, K. Lee, O. Mousis, A possible carbon-rich interior in super-Earth 55 Cancri e. *Astrophys. J.* **759**, L40 (2012).
39. G. F. Davies, A. M. Dziewonski, Homogeneity and constitution of the earth's lower mantle and outer core. *Phys. Earth Planet. Inter.* **10**, 336–343 (1975).
40. G. Kresse, J. Furthmüller, Efficient iterative schemes for ab initio total-energy calculations using a plane-wave basis set. *Phys. Rev. B Condens. Matter* **54**, 11169–11186 (1996).
41. J. P. Perdew *et al.*, Restoring the density-gradient expansion for exchange in solids and surfaces. *Phys. Rev. Lett.* **100**, 136406 (2008). Correction in: *Phys. Rev. Lett.* **102**, 039902 (2009).
42. Y. Le Page, P. Saxe, Symmetry-general least-squares extraction of elastic data for strained materials from ab initio calculations of stress. *Phys. Rev. B Condens. Matter* **65**, 104104 (2002).
43. R. Hill, The elastic behaviour of a crystalline aggregate. *Proc. Phys. Soc. A* **65**, 349–354 (1952).
44. N. Dubrovinskaia, L. Dubrovinsky, R. Caracas, M. Hanfland, Diamond as a high pressure gauge up to 2.7 Mbar. *Appl. Phys. Lett.* **97**, 251903 (2010).